



## Determination of Electrical Properties and Microhardness of Fe-Mn-Ti-Sn Heusler Composition

Mehtap Payveren Arıkan<sup>a</sup>, Fermin Ak<sup>\*b</sup>, Buket Saatçi<sup>c</sup>

<sup>a</sup>Faculty of Dentistry, Erciyes University, Kayseri, 38039, Türkiye

<sup>b</sup>Department of Medical Services and Techniques, Darende Bekir Ilıcak Vocational School, Malatya Turgut Özal University, 44700, Malatya, Türkiye

<sup>c</sup>Department of Physics, Erciyes University, Kayseri, 38039, Türkiye

\* Corresponding author: E-mail: [fermin.ak@ozal.edu.tr](mailto:fermin.ak@ozal.edu.tr)

### ABSTRACT

Fe-Mn-Ti-Sn alloy is a Heusler-type shape memory alloy; however, studies focusing on its electrical conductivity and microhardness are limited. In the study, Fe-Mn-Ti-Sn Heusler [Fe<sub>2-x</sub>Mn<sub>x</sub>TiSn (0 ≤ x ≤ 2)] alloy was selected Fe<sub>2</sub>TiSn, Fe<sub>1.5</sub>Mn<sub>0.5</sub>TiSn, FeMnTiSn, Fe<sub>0.5</sub>Mn<sub>1.5</sub>TiSn, Mn<sub>2</sub>TiSn components were obtained in these ratios for the first time using arc melter melting furnace. Temperature dependent electrical measurements of the obtained samples were determined by four point probe method (FPPT). The electrical resistance values of the samples at 330K were obtained as 0.14-2.25x10<sup>-6</sup> (□m) and 0.02-0.49 x10<sup>-6</sup> (□m) at 750 K. In addition, the temperature coefficient of electrical resistivity value was calculated as □□ (0.03-1.29)x (10<sup>-3</sup> K<sup>-1</sup>). Phases belonging to each composition were determined by examining the XRD peaks. Microstructures of the samples were obtained by SEM, EDX and MAPPING images. Finally, the composition-dependent microhardness measurements of the samples were determined by using the Vickers hardness test. The average microhardness values obtained were measured as 481-716 HV0.5.

### ARTICLE INFO

**Keywords:**

Four Point Probe Technique,  
Heusler alloys,  
Vickers Hardness

**Received:** April 19, 2025

**Accepted:** May 8, 2025

**ISSN:** 2651-3080

**DOI:** 10.54565/jphcfum.1680077

### 1. INTRODUCTION

Heusler alloys have been known for over a century and have attracted great attention due to their potential applications in new magnetic materials such as magnetic field-induced shape memory [1,2]. Today, two classes of materials are called Heusler alloys: semi-Heusler alloys with the general formula XYZ and full-Heusler alloys with the general formula X<sub>2</sub>YZ (where X and Y are transition metals and Z is an element of subgroups III-IV). Heusler-type compounds have been extensively studied in the fields of semiconductors, semimetals, ferromagnets, antiferromagnets, etc. Due to their different physical properties and practical applications. A wide range of physical properties have been observed in Heusler-type compounds. Since Heusler alloys mostly exhibit high magnetic properties, there are enough studies in the literature on this subject and new studies are added to these studies every day. However, when these existing studies are examined, few studies on their electrical and mechanical

properties are found. Fe-Sn-Ti eutectic alloy, one of the Heusler alloys, also has potential use in automotive, aerospace and biomedical applications due to its good mechanical properties [3].

Despite the rich body of literature devoted to the magnetic behaviour of Heusler alloys, systematic correlations between their electrical transport, micro-/nano-scale mechanical strength, and underlying phase constitution remain scarce—especially for the quaternary Fe–Mn–Ti–Sn system. In the present work, we provide the first integrated investigation that (i) synthesises Fe–Mn–Ti–Sn full-Heusler alloys via arc-melting under identical thermal histories, (ii) maps temperature-dependent resistivity, Hall coefficients, and magnetoresistance across 10–300 K, and (iii) quantifies microhardness and elastic modulus using instrumented indentation, linking both transport and mechanical responses to microstructural features revealed by XRD and SEM/EDS. By bridging these usually isolated property domains, our study establishes a

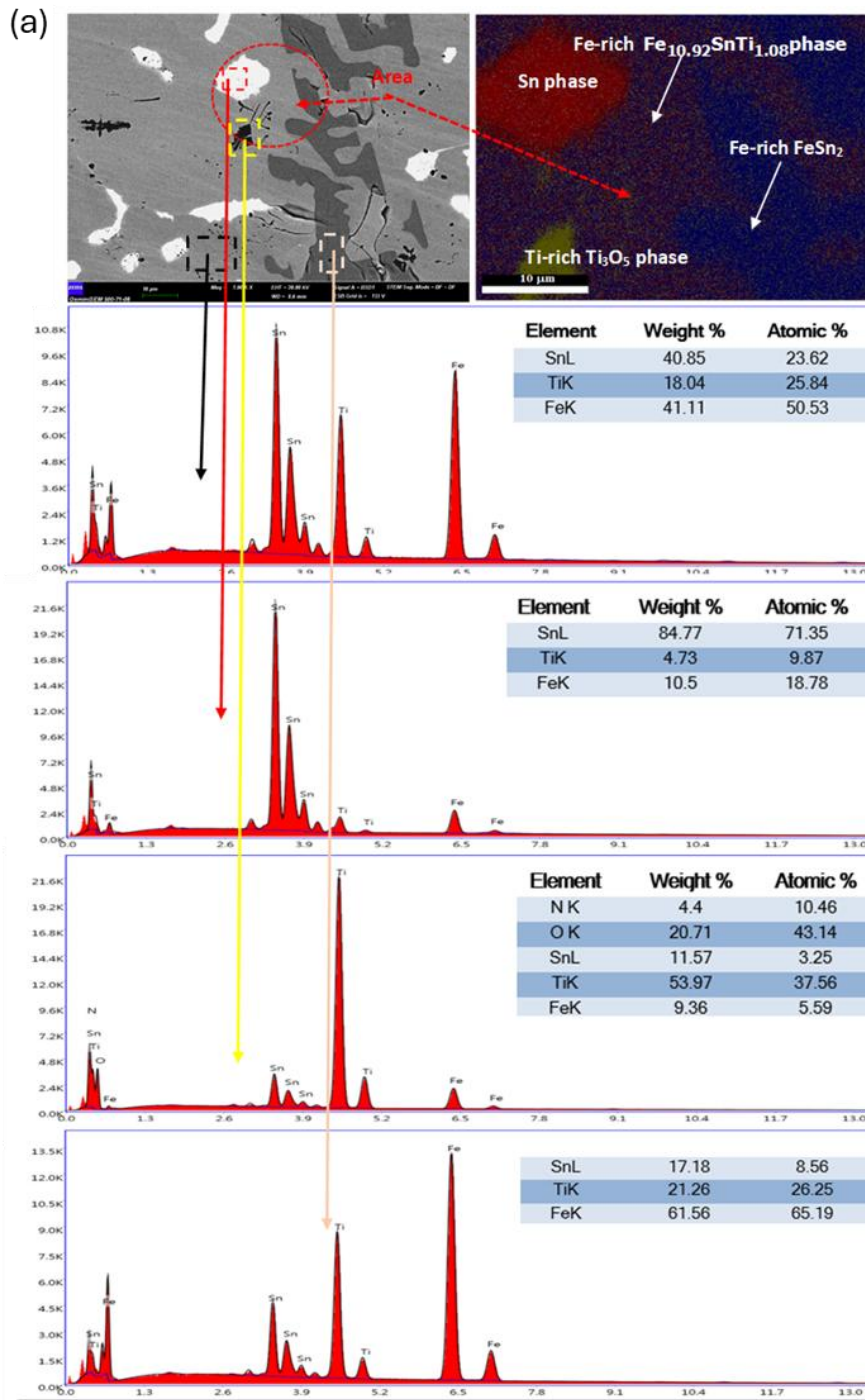
comprehensive property matrix that can guide alloy design for multifunctional applications in automotive, aerospace, sensors, and biomedical sectors, thereby adding a genuinely new dimension to the existing Heusler-alloy knowledge base.

## 2. MATERIAL AND METHOD

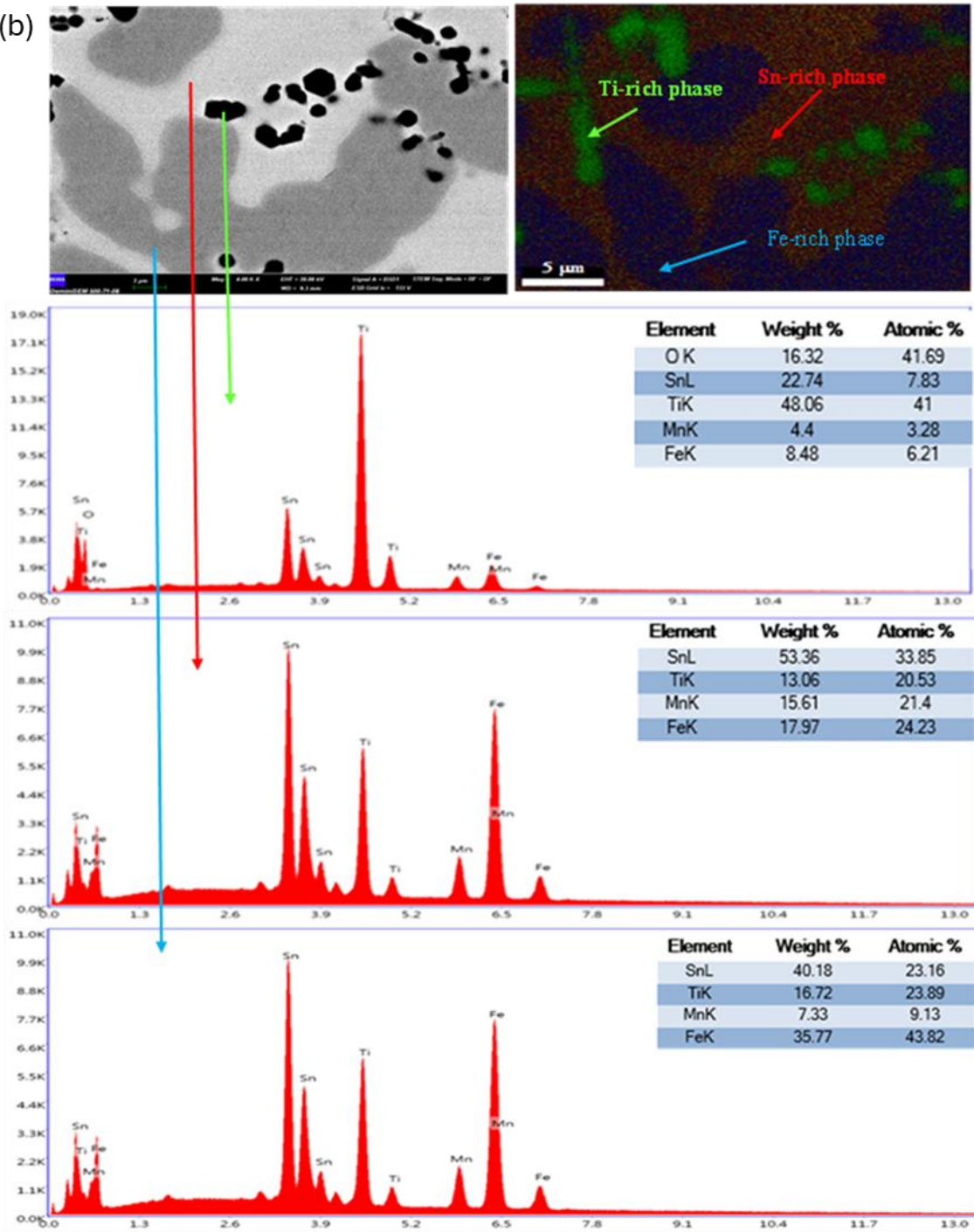
Within the scope of this project, Fe-Mn-Ti-Sn Heusler alloys were investigated. In the study, the desired stoichiometric amounts of high-purity Fe(99.5%) , Mn (99.95%), Ti(99%) and Sn(99.9% ) elements [ $\text{Fe}_{2-x}\text{Mn}_x\text{TiSn}$  ( $0 \leq x \leq 2$ )] were weighed on a precision balance and mixed in an Agate mortar for 30-40 minutes to make them homogeneous. The powder sample was compressed under 20 bar pressure. The samples, which were turned into pellets, were melted in a water-cooled copper crucible at under argon atmosphere using the Edmund Bühler Arc Melter AM brand (for samples with a melting point of up to approximately 4000 °C) melting furnace method to provide the desired Heusler conditions. The melting process was repeated several times to ensure that the samples were homogeneous. During melting, water was passed through the copper crucible to absorb the heat generated in the

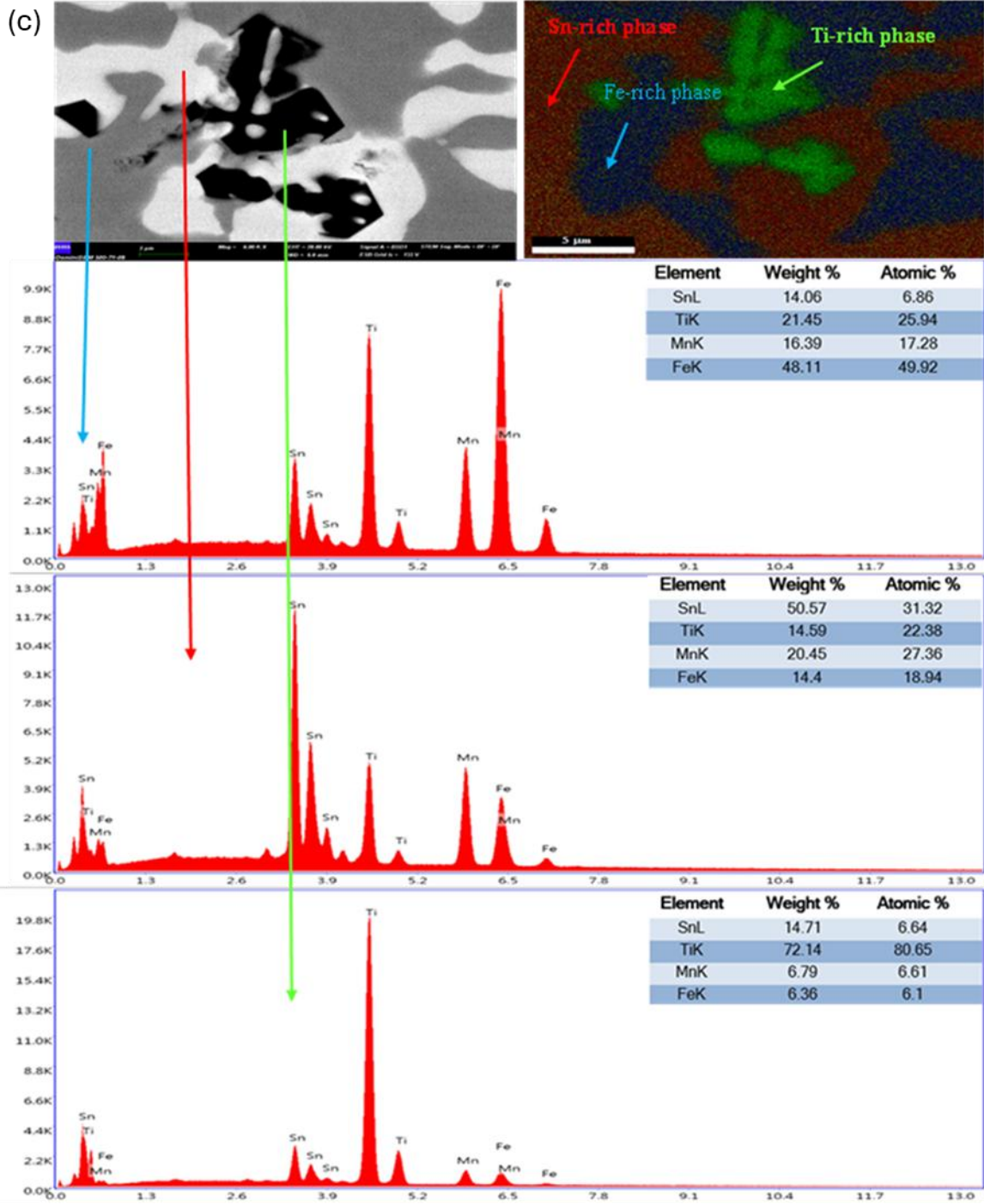
copper crucible and to prevent the copper from contaminating the material resulting from melting, and the melting process was carried out under an argon atmosphere to prevent oxidation of the samples.

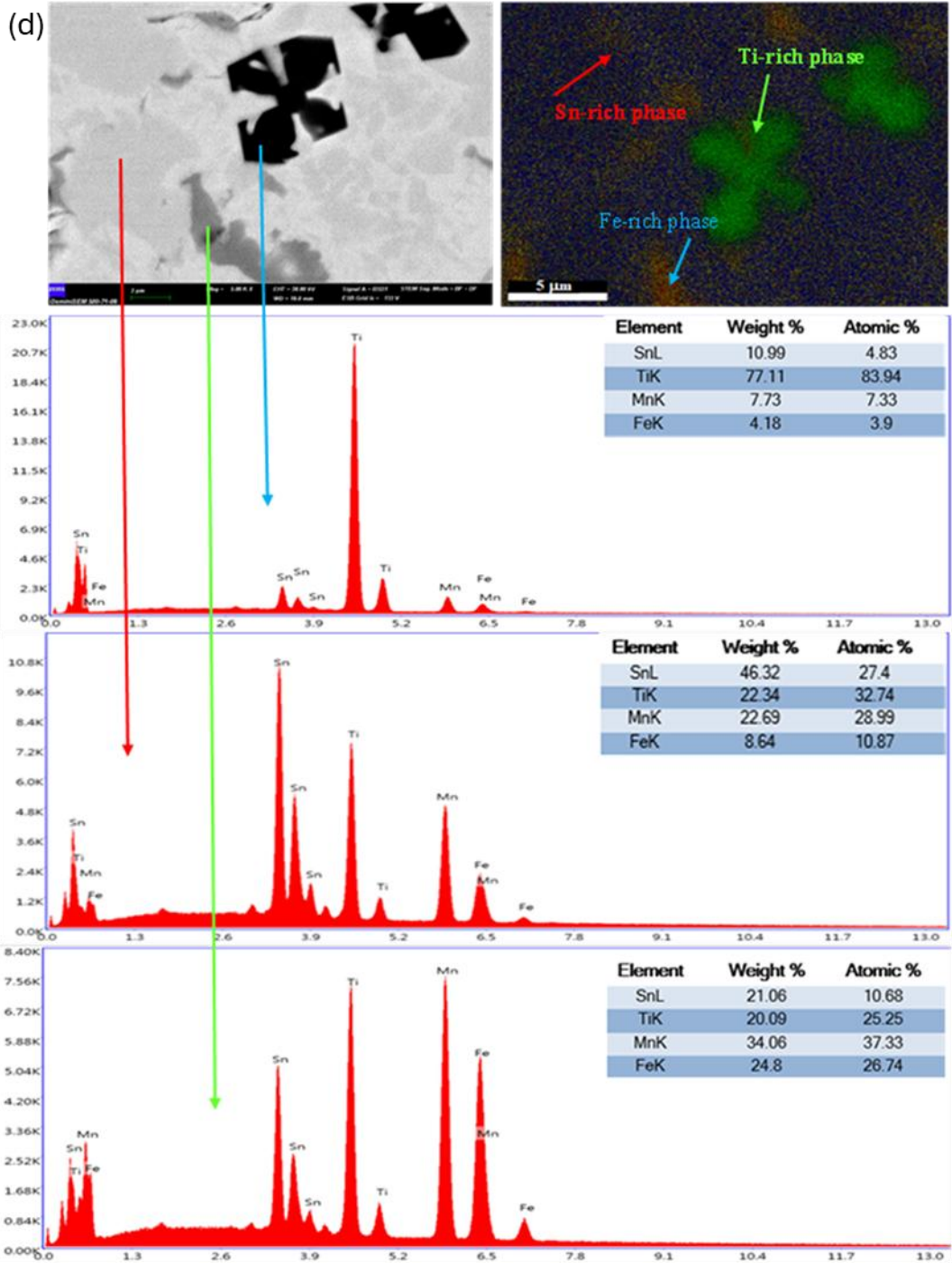
Then, the obtained samples were cut into small pieces with a minitom brand cutting device and some parts were molded. XRD, SEM, EDX and MAPPING images were taken from these molded parts. The XRD analysis of samples was carried out by a PANalytical Empyrean Model Diffractometer at room temperature using Cu-K $\alpha$  radiation with a wavelength of 1.54 Å and a scanning step of 0.02 °/sec. The thallium-activated sodium iodide detector (NaI) scintillation counter picked X-rays scattered from distinct atomic planes. The Win-Index and X-Powder software were employed for assessing XRD patterns and determining crystal structure characteristics such as crystal size and microstrain. The morphological properties of the obtained samples were investigated using Backscattered Electron (BSE) in a ZEISS Gemini SEM 500 model Field Emission Scanning Electron Microscope (FE-SEM), in Figure 1a,1b,1c,1d and 1e.



(b)







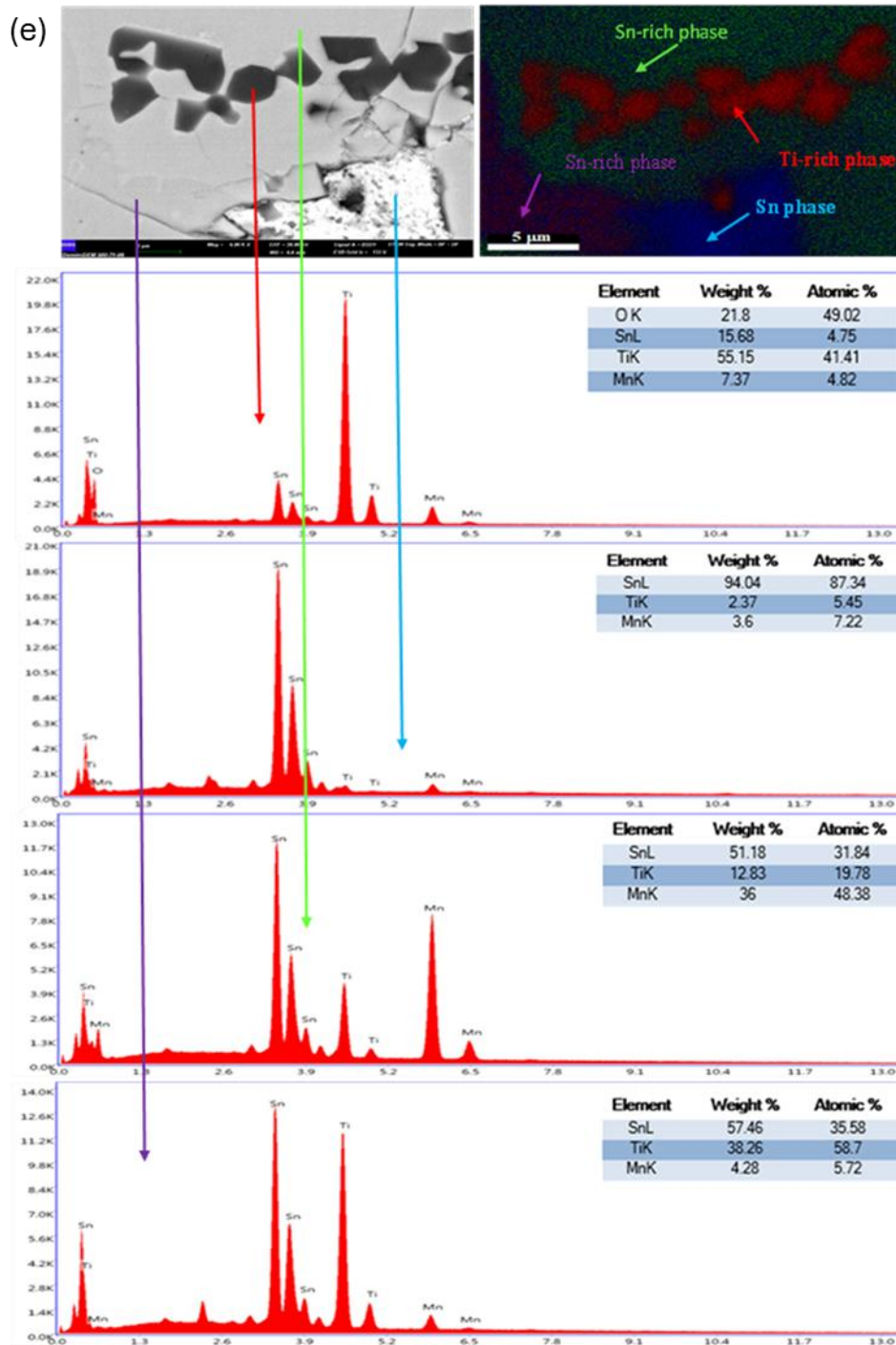


**Figure 1.** SEM, EDX and Mapping images of the samples (a)  $\text{Fe}_2\text{TiSn}$  (b)  $\text{Fe}_{1.5}\text{Mn}_{0.5}\text{TiSn}$  (c)  $\text{FeMnTiSn}$  (d)  $\text{Fe}_{0.5}\text{Mn}_{1.5}\text{TiSn}$  (e)  $\text{Mn}_2\text{TiSn}$ .

Other parts with the same composition were used in the microhardness device and the four-point probe electrical measurement device. The microhardness of the samples was measured with the Emno Test Brand Duroscan Model microhardness measurement device at Erciyes University Technology Research and Application Center. A Vickers Hardness tip was used in the measurements and according to the Vickers hardness measurement principle, it was measured under a load of 500 g in 15 seconds. To keep the error limit low, at least four measurements were taken

from each sample and their average was calculated. Track trace image evaluations on the device can be made directly on a screen on the device using software. The device table on which the sample is placed can be moved in the x-y axis with micrometer precision. Screenshots were taken only for some samples. The electrical conductivity values depending on the temperature of all specimens were measured with the Four Point Probe Technique (FPPT), which allows for accurate conductivity testing without the presence of any additional resistivity, such as contact resistance. The

conductivity experiments were conducted in a set-up muffle furnace using a specifically designed alumina kit frame, a Keithley 2700 type multimeter, and a Keithley 2400 version D.C. power supply. Two current and two voltage channels of four platinum probes, each aligned at a distance of 0.20 cm, touched down on the samples placed in

the kit system. Then, all data were transferred to the digitally controlled computer using the General Purpose Interface Bus (GPIB) certified electronic digital interface card. The furnace temperature was gradually increased from room temperature to a high temperature (1000 °C) by using a consistent heating step (10 °C /min) (Table 1).

**Table 1** Electrical properties at 330 K and 750 K for the Fe-Mn-Ti-Sn Heusler Alloy

Samples	Electrical Resistivity $\rho$ $10^{-6}$ ( $\Omega\text{m}$ )		The temperature
	T = 330 K	T = 750 K	coefficient of electrical resistivity, $\alpha_\rho$ ( $10^{-3} \text{ K}^{-1}$ )
			$\Delta T = 330 \text{ K} - 750 \text{ K}$
Fe <sub>2</sub> TiSn	2.09	0.49	0.57
Fe <sub>1.5</sub> Mn <sub>0.5</sub> TiSn	0.47	0.06	1.29
FeMnTiSn	0.14	0.37	0.06
Fe <sub>0.5</sub> Mn <sub>1.5</sub> TiSn	2.25	0.02	0.03
Mn <sub>2</sub> TiSn	9.15	0.31	0.08

In addition, the temperature coefficient of resistivity (TCR),  $\alpha_\rho$ , of the Fe-Mn-Ti-Sn Heusler alloys was also estimated from the electrical resistivity results obtained in the temperature range 330-750 K by equation 1:

$$\alpha_\rho = \left(\frac{1}{\rho_1}\right) \left(\frac{d\rho}{dT}\right) = \left(\frac{1}{\rho_1}\right) \left(\frac{\Delta\rho}{\Delta T}\right) \quad (1)$$

where  $\alpha_\rho$  is the TCR in the temperature between  $\Delta T = T_2 - T_1$  and  $\Delta\rho = \rho_2 - \rho_1$ ,  $\rho_1$  is the resistivity at  $T_1$  and  $\rho_2$  is the resistivity at  $T_2$  [4].

### 3. RESULTS AND DISCUSSIONS

Four phase regions were observed in the Fe<sub>2</sub>TiSn sample (Sample 1) (Figure 1a). Fe, Ti, and Sn elements were used in the sample. However, the oxygen element entered the powder sample structure during sample preparation and

formed an intermetallic phase with the Ti element during melting at high temperatures. Titanium can form oxides in various forms such as TiO, TiO<sub>2</sub>, Ti<sub>2</sub>O<sub>3</sub>, and Ti<sub>3</sub>O<sub>5</sub> during melting at high temperatures, and the layer structures of these oxides are complex [5,6]. In this composition, the phase formed by titanium is the Ti<sub>3</sub>O<sub>5</sub> phase. Likewise, the oxygen structure in other intermetallic phases originates from the oxygen trapped in the sample during melting. The existence of these phases is shown in Figure 2 and it is also supported by XRD diffraction patterns. Again, if we look at the EDX analysis in the second graph in Figure 1a, Ti and Sn elements are also seen in the Sn phase. However, since these are below the background in the XRD peaks, the effective phase is Sn. This situation is shown in the figure as the Sn-rich phase. The tetragonal FeSn<sub>2</sub> phase obtained in Sample 1 also coincides with the literature [7].

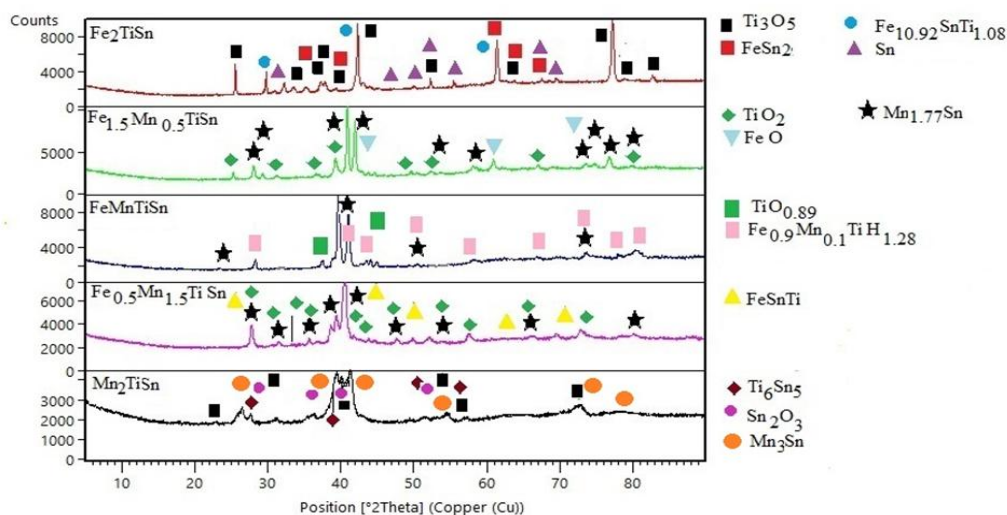


**Figure 2.** XRD diffraction patterns of all samples in Fe-Mn-Ti-Sn Alloys

Three intermetallic phases were observed in the Fe<sub>1.5</sub>Mn<sub>0.5</sub>TiSn sample (Sample 2) (Figure 1b). In this example, unlike the other one, the element Mn is used. In this study, the phase formed by titanium is the TiO<sub>2</sub> phase. Likewise, the oxygen structure in other intermetallic phases

originates from the oxygen trapped in the sample during melting. Additionally, the Mn<sub>1.77</sub>Sn phase is also present in the sample. The existence of these phases is also supported by XRD diffraction patterns in Figure 2. Since the oxygen element is not the selected element and is not expected to be

in the sample, oxygen in the 2nd graph in Figure 1b has been excluded from the EDX analysis. Eliminating oxygen caused the Sn phase to stand out more than it should in the mapping images in Figure-1b. However, since the Sn phase peaks were kept in the background, this phase was not observed in the XRD analysis. In the FeMnTiSn sample (Sample 3)(Figure 1c), all four elements were used in a 1-mole ratio, and three intermetallic phases were observed. In this compound, the phase formed by titanium is the cubic  $\text{TiO}_{0.89}$  phase. Additionally,  $\text{Fe}_{0.9}\text{Mn}_{0.1}\text{TiH}_{1.28}$  phase is also present. The existence of these phases is also supported by the XRD diffraction patterns in Figure 2. It is also estimated that the hydride phase forms by entering into an intermediate position during sample preparation at room conditions. Three intermetallic phases were observed in the  $\text{Fe}_{0.5}\text{Mn}_{1.5}\text{TiSn}$  sample (Sample 4)(Figure 1d). The phases and their regions are clear in the mapping in Figure 1d. The existence of phases is also supported by XRD diffraction patterns in Figure 2. Although three elements were used in the last sample,  $\text{Mn}_2\text{TiSn}$  (Sample 5)(Figure 1e), 4 intermetallic phases were observed and one of these phases

was the  $\text{Ti}_3\text{O}_5$  phase.  $\text{Ti}_3\text{O}_5$  phase was observed in both the first sample and the last sample. This situation was already expected due to the experimental conditions. In addition,  $\text{Mn}_3\text{Sn}$  and  $\text{Ti}_6\text{Sn}_5$  phases were observed and these phases obtained are compatible with similar studies in the literature [8]. The microhardness of the samples measured using the Vickers hardness test are shown in Table 2 and these images are given symbolically in Figure 3 using screenshots. Additionally, as it is known, as the dislocations in the sample increase, the hardness increases. The microhardness of materials is also related to their electrical properties. High hardness is observed in the layers with low electrical conductivity, and low hardness is observed between the planes with high electrical conductivity. The microhardness values obtained in the study were measured at room temperature. Electrical conductivity values were measured depending on temperature. Since microhardness values were measured at room temperature, a comparison was made with the electrical conductivity values at room temperature.

**Table 2.** The micro hardnesses of the samples measured using the Vickers hardness test

Sample No	Sample Name	Average (HV)
1	$\text{Fe}_2\text{TiSn}$	710
2	$\text{Fe}_{1.5}\text{Mn}_{0.5}\text{TiSn}$	705
3	$\text{FeMnTiSn}$	698
4	$\text{Fe}_{0.5}\text{Mn}_{1.5}\text{TiSn}$	716
5	$\text{Mn}_2\text{TiSn}$	481

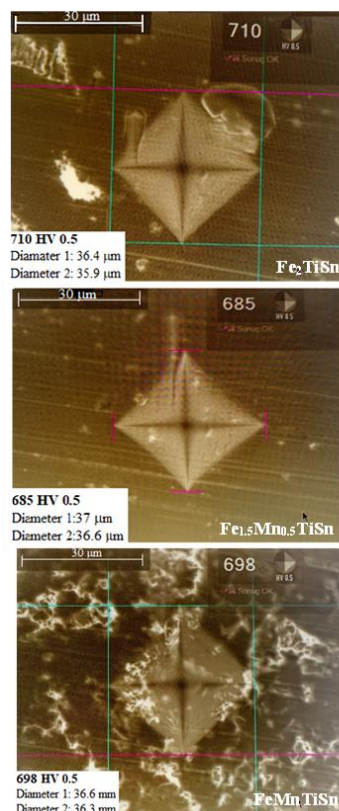


**Figure 3.** Representative images of some of the samples whose microhardness was measured using the Vickers hardness test.

In this comparison, the lowest microhardness value belongs to the  $\text{Mn}_2\text{TiSn}$  sample. But the highest electrical resistance value belongs to the  $\text{FeMnTiSn}$  sample, although it should belong to the same sample. This may be due to the 1:1:1 doping of the samples in the alloy and especially the higher hardness values of Ti and Fe elements compared to other elements. But the hardness value of this composition is not high enough because the Mn element is doped as  $\text{Mn}_2$  and has a low hardness value. Because of adding Fe element to the alloy, the microhardness value increased. As the composition of the Mn element decreased and the component of the Fe element increased, the hardness value increased depending on this ratio. The microhardness value of  $\text{Fe}_2\text{TiSn}$  remained at a medium value. There is a 2:1:1 ratio here, and the low microhardness value of Sn versus the high microhardness value of the Fe element and Ti element may have created such a situation. The electrical resistance values of all samples in the study are close to each other up to 800 K. This situation can be seen in Figure 4. After 800 K, there is an increase in the electrical resistance values of all samples. However, while this increase shows a smooth transition in some samples, it

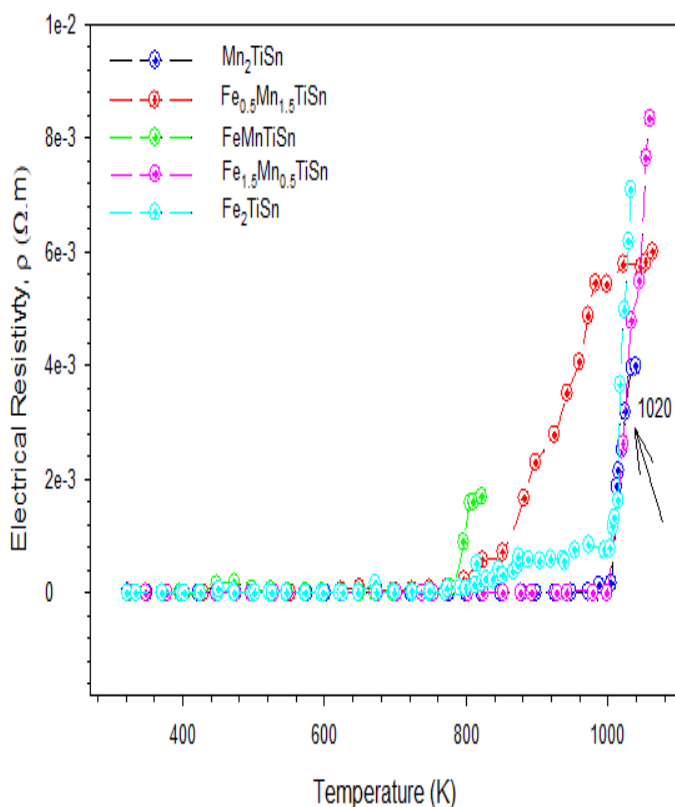


**Figure 4.** The electrical resistivities of Fe-Mn-Ti-Sn Heusler samples

manifests itself with a hard transition in some samples. The same ratios of Ti and Sn elements play a role in these hard transitions, especially in  $\text{FeMnTiSn}$ ,  $\text{Mn}_2\text{TiSn}$ , and  $\text{Fe}_{1.5}\text{Mn}_{0.5}\text{TiSn}$  samples. These soft transitions in the  $\text{Fe}_2\text{TiSn}$  and  $\text{Fe}_{0.5}\text{Mn}_{1.5}\text{TiSn}$  samples, which have soft transitions, are caused by the change in the iron ratio and adding the Mn element to the system. These differences are also seen in the microhardness values in Table 2. In addition, as seen in Figure 4, a sudden increase in electrical resistance is observed around 1020 K in samples numbered ( $\text{Fe}_2\text{TiSn}$ ) 1, ( $\text{Fe}_{1.5}\text{Mn}_{0.5}\text{TiSn}$ ) 2 and ( $\text{Mn}_2\text{TiSn}$ ) 5. The reason for this transition is due to the doping of Ti and Sn ratios at a ratio of 1:1 for all three samples and that Ti and Sn metal may cause such a transition or a second-degree phase transition may be possible [9]. When the results regarding the  $\text{Fe}_2\text{TiSn}$  composition were compared with the literature, it was seen that they agreed (Figure 5). However, since there were no appropriate electrical resistance results with the other compounds in the study, a comparison of other components with the literature could not be made. The results obtained from the components were compared with each other.

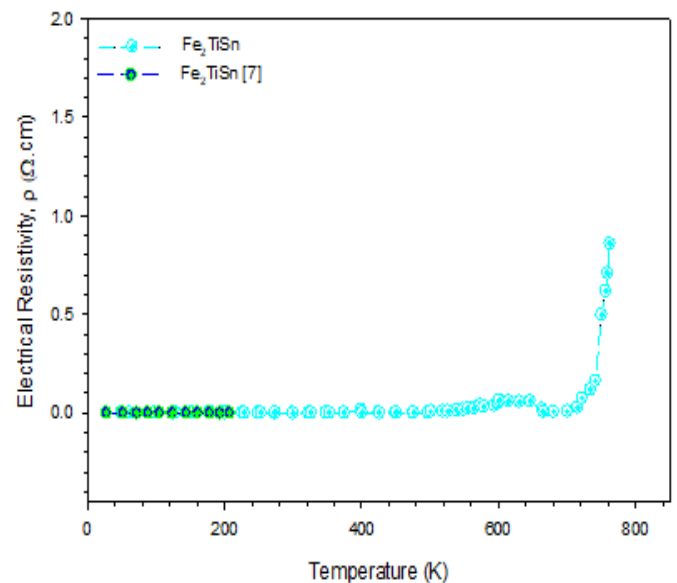


**Figure 5:** Literature comparison of electrical resistances [7]

**Acknowledgement:** We would like to thank the Proofreading & Editing Office of the Dean for Research at Erciyes University for the copyediting and proofreading service for this manuscript.

#### Competing interests

This article was financially supported by Malatya Turgut Özal University Scientific Research Projects Coordination Unit with project number 24H08. The authors are grateful to Malatya Turgut Özal University Research Foundation for their financial support.

## REFERENCES

- [1] Ullakko, K., Huang, J. K., Kantner, C., O'handley, R. C., & Kokorin, V. V. (1996). Large magnetic-field-induced strains in Ni<sub>2</sub>MnGa single crystals. *Applied Physics Letters*, 69(13), 1966-1968.
- [2] Kainuma, R., Imano, Y., Ito, W., Sutou, Y., Morito, H., Okamoto, S., ... & Ishida, K. (2006). Magnetic-field-induced shape recovery by reverse phase transformation. *Nature*, 439(7079), 957-960.
- [3] Lütjering, G., & Albrecht, (2003). *J. D GINI WILEY-VCH Verlag GmbH & Co. KGaA*.
- [4] Billur, C. A., Gerçekcioglu, E., Bozoklu, M., Saatçi, B., Ari, M., & Nair, F., (2015). The electrical, thermal conductivity, microstructure and mechanical properties of Al–Sn–Pb ternary alloys. *Solid State Sciences*, 46, 107-115.
- [5] Sartale, S. D., Ansari, A. A., & Rezvani, S. J. (2013). Influence of Ti film thickness and oxidation temperature on TiO<sub>2</sub> thin film formation via thermal oxidation of sputtered Ti film. *Materials science in semiconductor processing*, 16(6), 2005-2012.
- [6] Byun, J. M., Choi, H. R., Kim, S. H., Suk, M. J., & Do Kim, Y. (2017). Formation of nanostructured rutile TiO<sub>2</sub> synthesized on Ti powder via thermal oxidation. *Applied Surface Science*, 415, 43-48.
- [7] Saito, T., & Kamishima, S. (2018). Magnetic and thermoelectric properties of Fe–Ti–Sn alloys. *IEEE Transactions on Magnetics*, 55(2), 1-4.
- [8] Tkachuk, A. V., Akselrud, L. G., Stadnyk, Y. V., & Bodak, O. I. (2000). Isothermal section of the Ti–Mn–Sn system and crystal structure of the TiMnSn<sub>4</sub> compound. *Journal of alloys and compounds*, 312(1-2), 284-287.
- [9] Wang, Y., Yang, F., Shen, C., Yang, J., Hu, X., & Fei, Y. (2024). Electrical Resistivity and Phase Evolution of Fe–N Binary System at High Pressure and High Temperature. *Minerals*, 14(5), 467.